Supporting Information

Descriptors and graphical construction for in silico design of efficient and selective single atom catalysts for eNRR

Samadhan Kapse[a], Shobhana Narasimhan[b]*, Ranjit Thapa[a]**

[a]Department of Physics, SRM University – AP, Amaravati 522 502, Andhra Pradesh, India

[b]Theoretical Sciences Unit and School of Advanced Materials, Jawaharlal Nehru Centre for Advanced Scientific Research, Bangalore 560 064, Karnataka, India

*Corresponding Author: shobhana@jncasr.ac.in

**Corresponding Author: ranjit.t@srmap.edu.in

Contents

SI-1. Formation Energies (E_f) and dissolution potential (U_{diss}) of SACs.

SI-2. Density Functional Theory (DFT) calculations: Computational details

SI-3. Charge density difference analysis.

SI-4. Structures of the six types of model SACs.

SI-5. Thermodynamic and electrochemical stabilities for all 66 SACs.

SI-6. Study of dynamic stability of Mn-Pc system.

SI-7. Schematic diagram showing parameters determining optimal eNRR catalyst.

SI-8. Free energy profile for nitrogen reduction reaction for (a) Sc-Pc (b) Mn-Pc (c) Cr-N_4 (d) Fe-N_2C_2 SACs.

SI-9. Schematic diagram of steps in the nitrogen reduction reaction, for alternating and distal pathways.

SI-10. Free energy profile comparison between side-on and end-on N_2 adsorption pathways.

SI-11. Free energy profile of N_2 and NNH adsorption on metal centers of TM-N_XC_Y and TM-N_3 systems.

SI-12. Free energy profile of N_2 and NNH adsorption on the N, C sites of Sc-Pc and Sc-N_4 systems.

SI-13. Free energy profile of N_2 and NNH adsorption on the N, C sites of Sc-N_3 and Pc systems.

SI-14. Free energy profile of N_2 and NNH adsorption on the N, C sites of Co-Pc and Ni-Pc systems.

SI-15. Free energy profile of N_2 and NNH adsorption on the Sc-Pc (Cl) and V-Pc (Cl) SACs.

SI-16. Graph of η_{NRR} versus d band center and Bader charge.

SI-17. Comparison of charge density differences in Mn-Pc, Mn-N_XC_Y and Mn-N_3 systems.

SI-18. Comparison of charge density differences in TM-Pc systems with various metal centers.

SI-19. The ΔG_{NNH*} Vs N-N bond length.

SI-20. Charge density difference plots for N_2 adsorbed on different metal centers in TM-Pc.

SI-21. Free energy profile of the hydrogen evolution reaction for all 66 SACs.

SI-22. Comparison of (a) $\Delta G_{N_2^*}$ and (b) ΔG_{NNH^*} for all metal centers of all 66 SACs.

SI-23. Flowchart of catalyst screening process.

SI-24: Full free energy profile of eNRR on Cr-N_4 with and without water solvation effect.

SI-25. Table of values of computed parameters for SACs.

SI-26. The values of $\Delta G_{N_2^*}$ with end-on and side-on configuration on the metal site of all 66 SACs.

SI-27. The N-N bond length after adsorption on SACs.

SI-28. The comparison of NH_3 yield and FE of SACs by using reported experimental studies.

SI-29. Values of U_{diss}, U^0_{diss}, $and\ n$.

SI-30. References

SI-1. Formation Energies (E_f) and dissolution potential (U_{diss}) of SACs.

a. The formation energy (E_f) of TM-Pc SACs is calculated using the equation,

$$E_f = E_{\text{TM-Pc}} - (4*E_{\text{phthalonitrile}} + E_{\text{TM}})$$

where $E_{\text{TM-Pc}}$, $E_{\text{phthalonitrile}}$, and E_{TM} are the total energies of TM-Pc SACs, phthalonitrile system, and transition metal atom energy, respectively. For TM energy, we consider the total energy of bulk system and also the energy of single metal atom in a box as reference.

b. The formation energy (E_f) of TM-N_XC_Y SACs is calculated using the equation,

$$E_f = E_{\text{TM-NxCy}} + x\mu_{\text{H}} + y\mu_{\text{N}} - (E_{\text{Ph-btpy}} + z\mu_{\text{C}} + E_{\text{TM}})$$

where $E_{TM-NxCy}$, $E_{Ph\text{-}btpy}$, and E_{TM} are the total energies of TM-N_XC_Y SACs, Ph-btpy compound, and transition metal atom energy (bulk/adatom), respectively. Here μ_C is the chemical potential of a single C atom in Ph-btpy system, μ_H and μ_N are the chemical potentials of half of the hydrogen and nitrogen molecules energy in gas phase respectively. The x is the number of hydrogen atoms remains, y is the number of nitrogen atoms remains and, z is the number of carbon atoms replaced in SACs.

The dissolution potential (U_{diss}) of SACs is calculated using the equation,

$$U_{diss} = U^0_{diss} - {E_f}/{ne},$$

where, U^0_{diss} ,n, e are the standard dissolution potential of bulk metal, number of electrons, electron charge respectively. The exact values of U^0_{diss} ,n and U_{diss} (bulk metal as well as adatom) for all 66 SACs are listed in **Table S5**.

SI-2. Density Functional Theory (DFT) calculations: Computational Details

The first principles calculations were performed using density functional theory (DFT) as implemented in the Vienna Ab initio Simulation Package (VASP) [1]. Exchange-correlation interactions were treated using the Perdew-Burke-Ernzerhof (PBE) form of the Generalized Gradient Approximation (GGA) [2] and interactions between the ion cores and valence electrons were described using projector-augmented wave (PAW) pseudopotentials. The cut-off energy for the plane-wave basis was set equal to 450 eV. The convergence thresholds for total energies and forces were set at 1×10^{-6} eV and 0.01 eV/Å, respectively. The Brillouin zone was sampled at the Γ point only. The spin polarized DFT calculations are performed for all the systems[3,4]. Spurious interactions between repeating images were avoided by using a vacuum spacing of 15 Å in all directions.

The free energy profiles were used to estimate the theoretical overpotential that defines the performance of a catalyst for the nitrogen reduction reaction (NRR). The Gibbs free energies G were calculated by using the formula, $G = E + \mathrm{ZPE} - TS - neU$, where E is the DFT total energy, ZPE is the zero-point energy, TS is the entropic term, n is the number of electrons transferred and U is the potential applied at the electrode [5]. Here, we assumed that the TS and ZPE terms for adsorbed atoms/ions are negligible compared to the corresponding terms for the gaseous phase at room temperature and ambient pressure. The values of entropies and zero-point energies for the free molecules were obtain from a chemical database (https://janaf.nist.gov.). The PWscf package of the Quantum ESPRESSO distribution was used for charge density difference analysis of the SACs [6].

SI-3. Charge density difference analysis

The values obtained for adsorption energies were found to depend on the coordination configuration and type of metal center. We therefore plotted isosurfaces of the charge density difference to visualize the effect of coordination configuration on the metal center. As an example, for the Mn-Pc SAC, the charge density difference (Δρ) is computed using:

$$\Delta\rho = \rho\,(\text{Mn-Pc}) - \rho\,(\text{Pc}) - \rho\,(\text{Mn atom});$$

here the three terms on the right-hand side are the electronic charge densities, as computed from DFT, of Mn-Pc, the Pc alone (with the Mn center removed) and an isolated Mn atom in the gas phase.

We show here that Δρ can be tuned by varying either the coordination environment of the metal center, or the metal center itself, or both. In **Figure S14**, we show results for Δρ when the Mn atom is embedded in different coordination configurations. The small accumulation of localized charge can be the reason for moderate binding energy of NNH on Mn-Pc and Mn-N_XC_Y that leads to optimal eNRR activity and no H poisoning [7]. In contrast, the stronger adsorption in the Mn-N_3 system may arise from high localized charge accumulation on the metal center. Thus, the charge accumulation on the Mn center depends on its coordination configuration, and is responsible for changes in the adsorption properties in different SACs systems, even when the metal atom is the same [8]. In **Figure S15,** we demonstrate how the charge density difference can be tuned by varying the metal center in phthalocyanine.

SI-4. Structures of the six types of model SACs

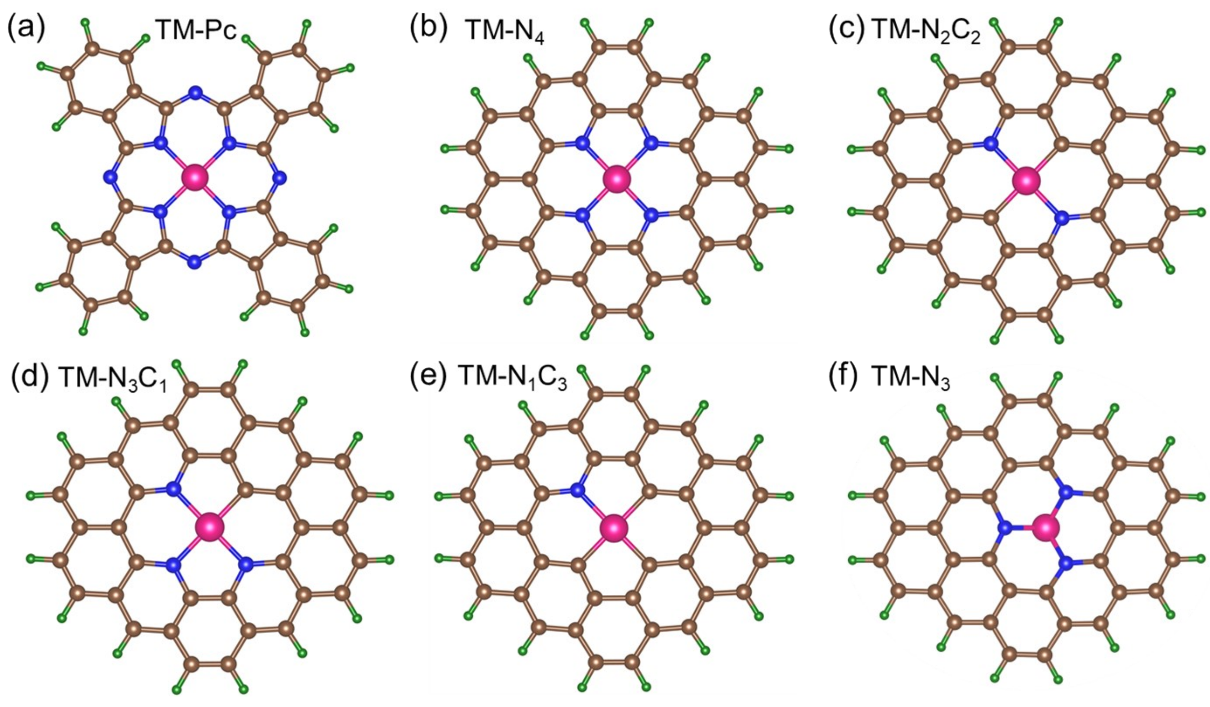

Figure S1: Structures of (a) TM-Pc (b) TM-N_4 (c) TM-N_2C_2 (d) TM-N_3C_1 (e) TM-N_1C_3 and (f) TM-N_3. The pink-, blue-, brown-, and green-colored spheres represent the transition metal, nitrogen, carbon and hydrogen atoms, respectively.

SI-5. Thermodynamic and electrochemical stabilities for all 66 SACs.

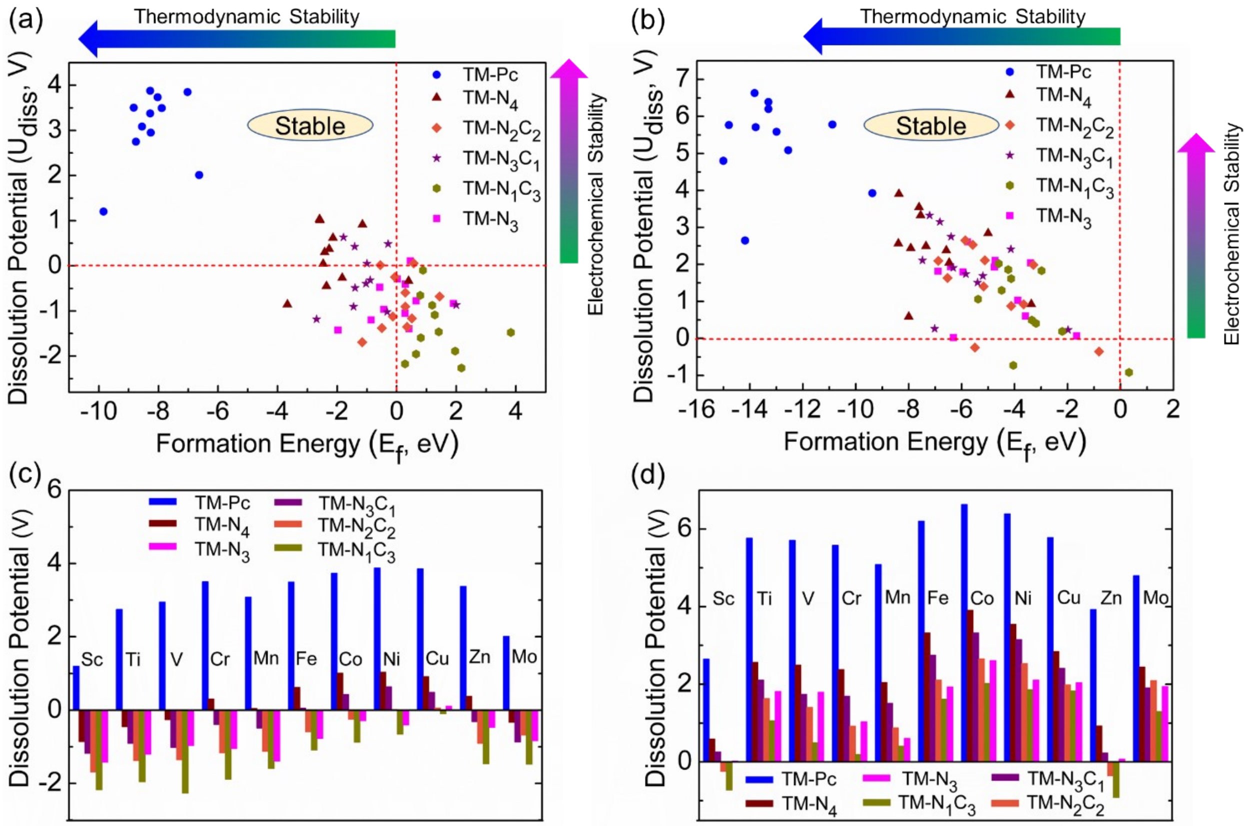

Figure S2: Plotting of the thermodynamic and electrochemical stabilities for all 66 single atom catalysts, upon considering source of metal atoms as (a) bulk, and (b) adatom. Computed results of dissolution potential for all 66 single atom catalysts, upon considering source of metal atoms as (c) bulk, and (d) adatom.

SI-6. Study of dynamic stability of Mn-Pc system.

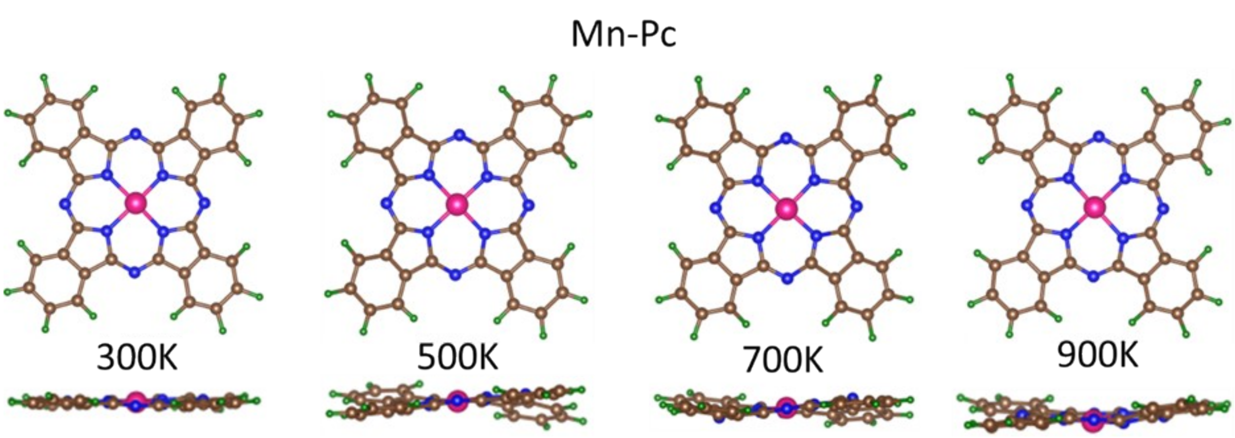

Figure S3: Optimized models of Mn-Pc molecule at different temperatures in molecular dynamics.

SI-7. Schematic diagram showing parameters determining optimal eNRR catalyst

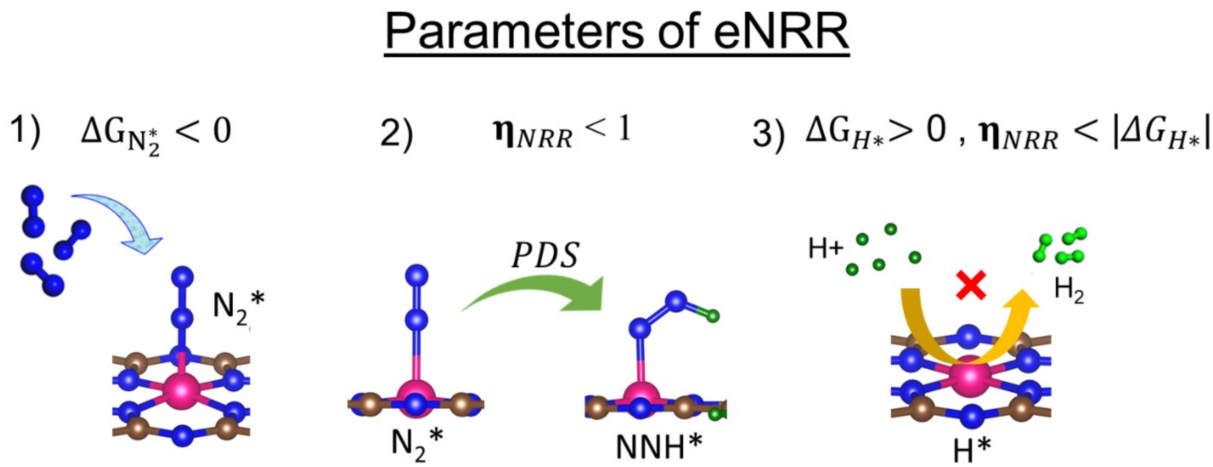

Figure S4: Schematic diagram representing the three parameters determining an optimal eNRR catalyst.

SI-8. Free energy profile for nitrogen reduction reaction for (a) Sc-Pc (b) Mn-Pc (c) Cr-N_4 (d) Fe-N_2C_2 SACs.

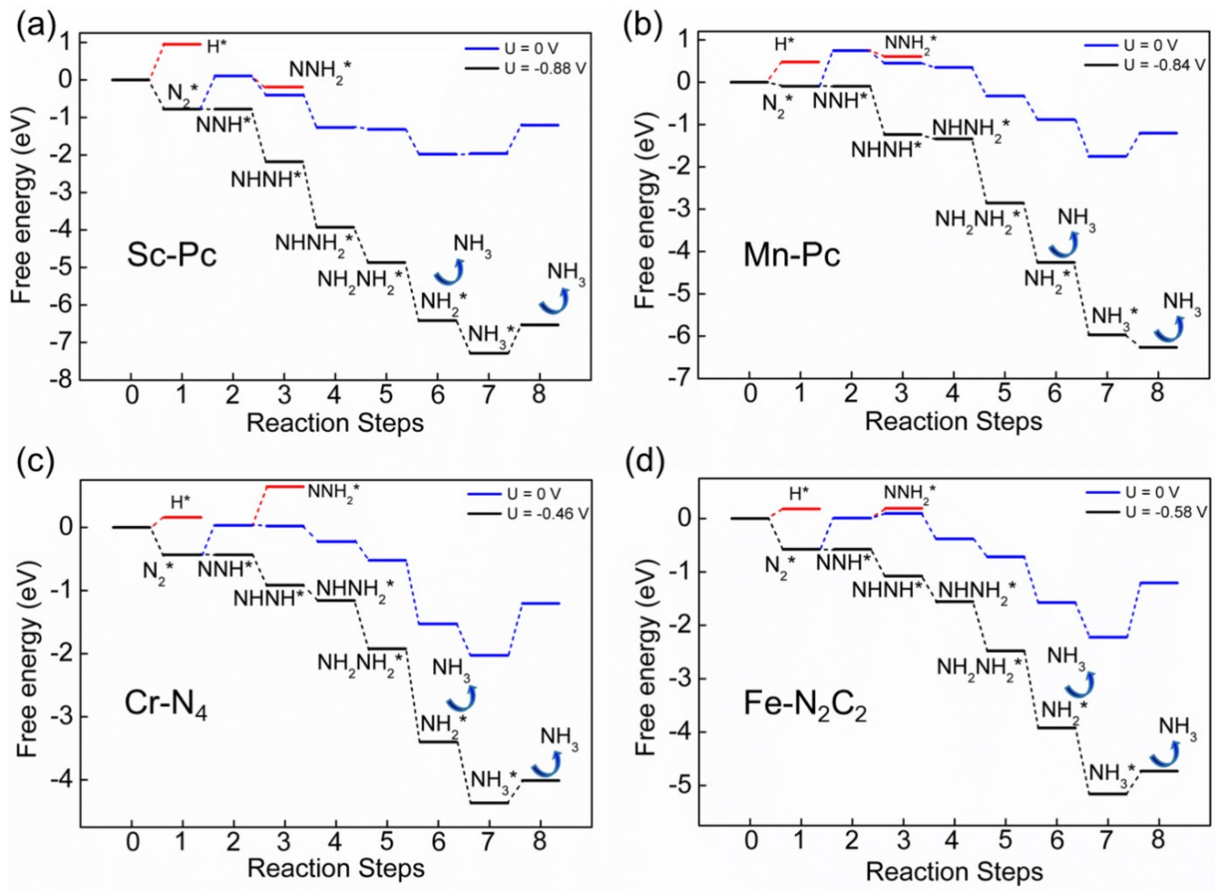

Figure S5: Computed free energy profiles for nitrogen reduction reaction for (a) Sc-Pc (b) Mn-Pc (c) Cr-N_4 (d) Fe-N_2C_2 systems. Here we consider the preferred alternating pathway at $U = 0$ V and at negative applied electrode potential (where all reaction steps become downhill) for each system. The oblique dotted lines are a guide to the eye.

SI-9. Schematic diagram of steps in the nitrogen reduction reaction, for alternating and distal pathways.

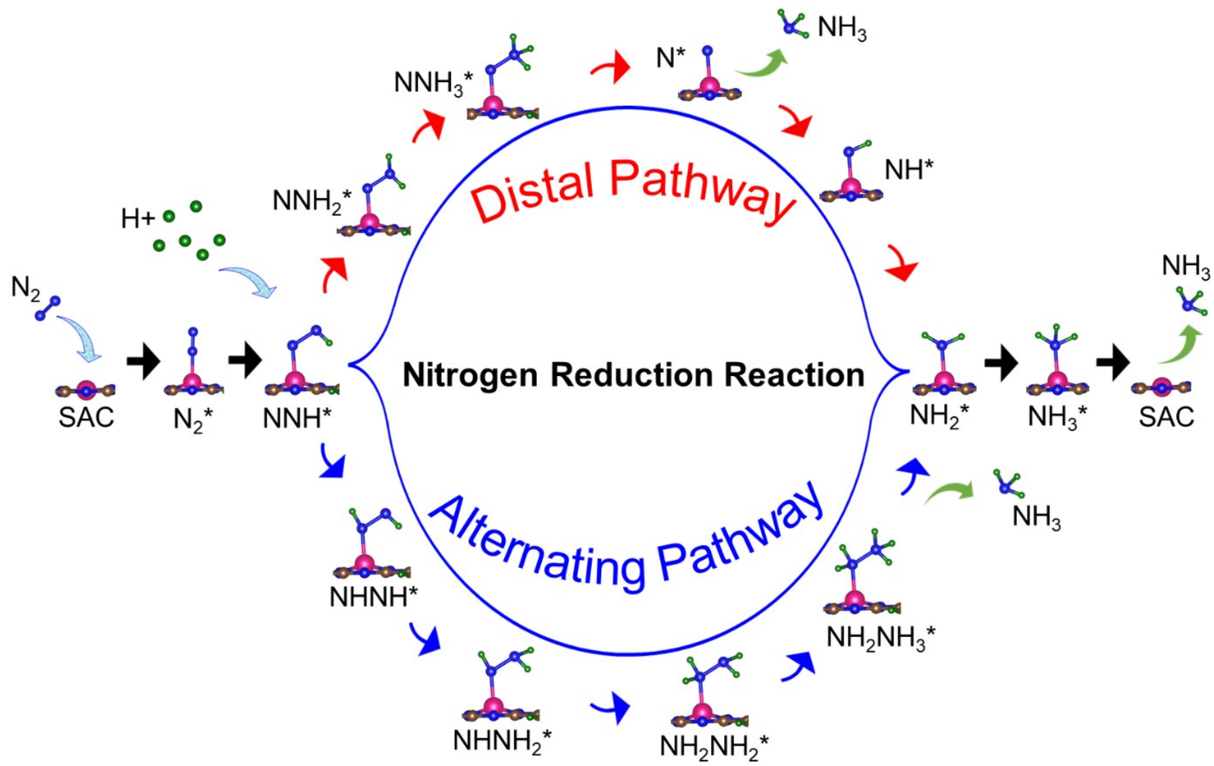

Figure S6: Schematic diagram shows the various steps of the nitrogen reduction reaction on the metal center of a SAC, via the alternating and distal pathways. The transition metal center, nitrogen, carbon and hydrogen atoms are denoted using pink, blue, brown, and green colored spheres, respectively. The * symbol denotes an adsorbed species.

SI-10: Free energy profile comparison between side-on and end-on N_2 adsorption pathways.

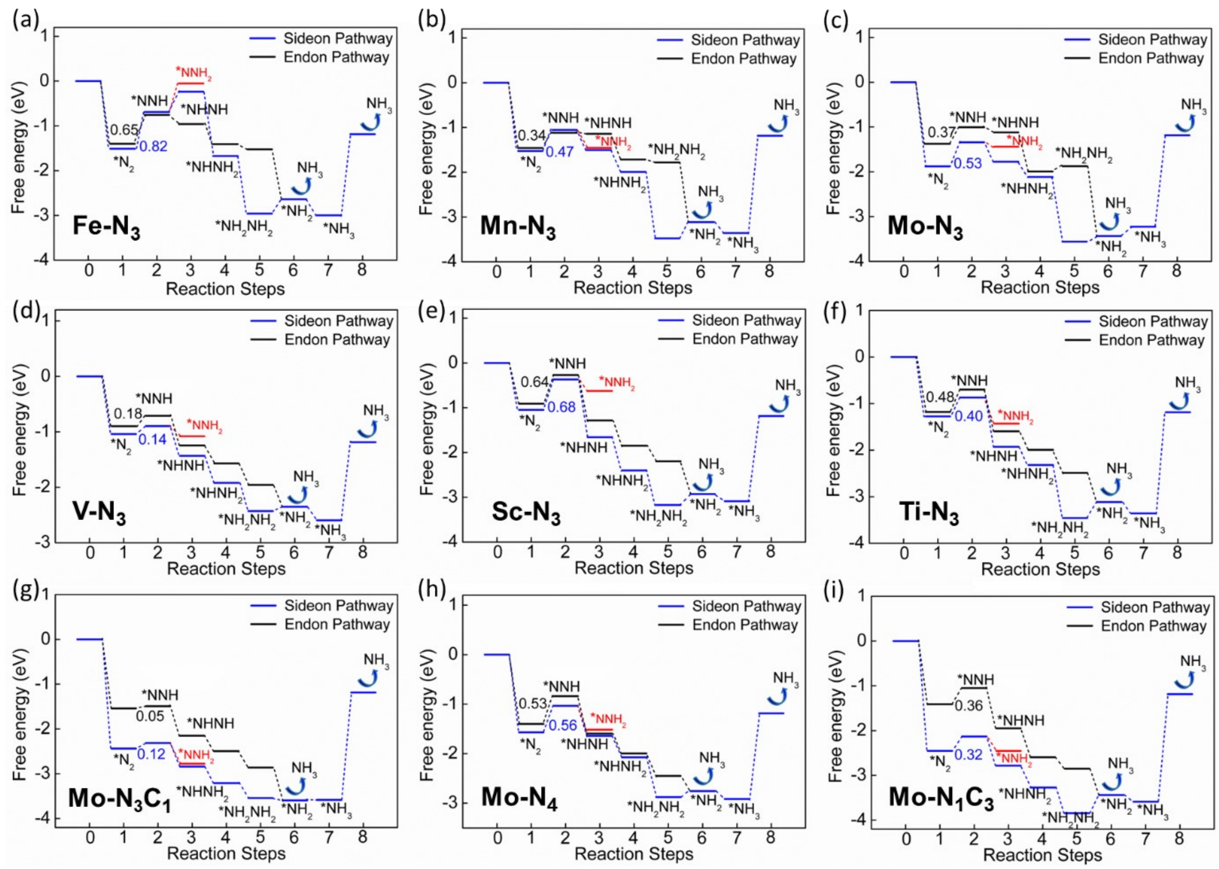

Figure S7 Comparison of free energy profile between side-on and end-on pathways on (a) Fe-N_3 (b) Mn-N_3 (c) Mo-N_3 (d) V-N_3 (e) Sc-N_3 (f) Ti-N_3 (g) Mo- N_3C_1 (h) Mo-N_4 (i) Mo- N_1C_3 systems.

SI-11. Free energy profile of N_2 and NNH adsorption on metal centers of TM-N_XC_Y and TM-N_3 systems.

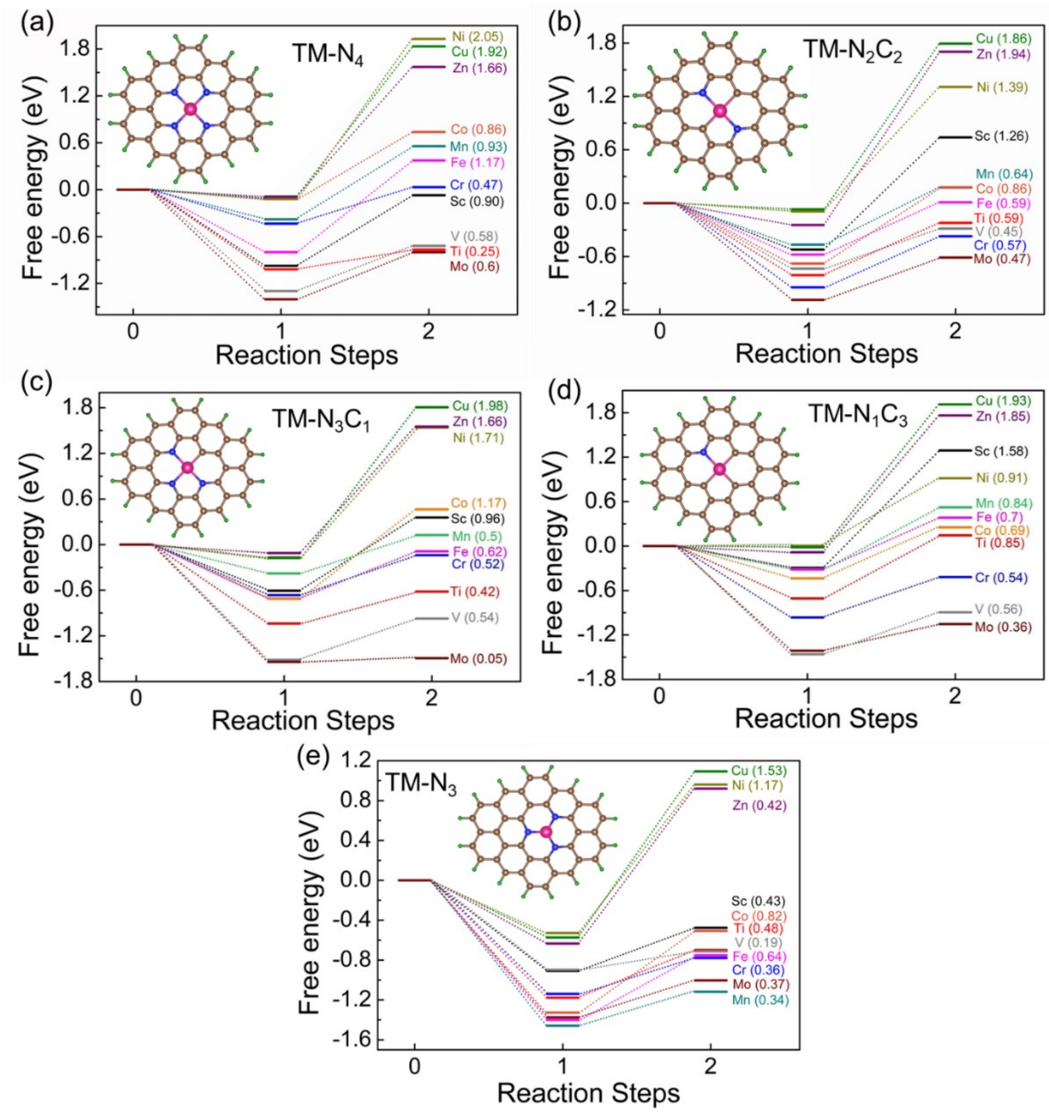

Figure S8: Computed free energy profiles of N_2 and NNH adsorption on various metal center of (a) TM-N_4 (b) TM-N_2C_2 (c) TM-N_3C_1 (d) TM-N_1C_3 and (e) TM-N_3. The values listed in parentheses indicate the corresponding values of η_{NRR}. The dotted lines are a guide to the eye.

SI-12. Free energy profile of N_2 and NNH adsorption on the N, C sites of Sc-Pc and Sc-N_4 systems.

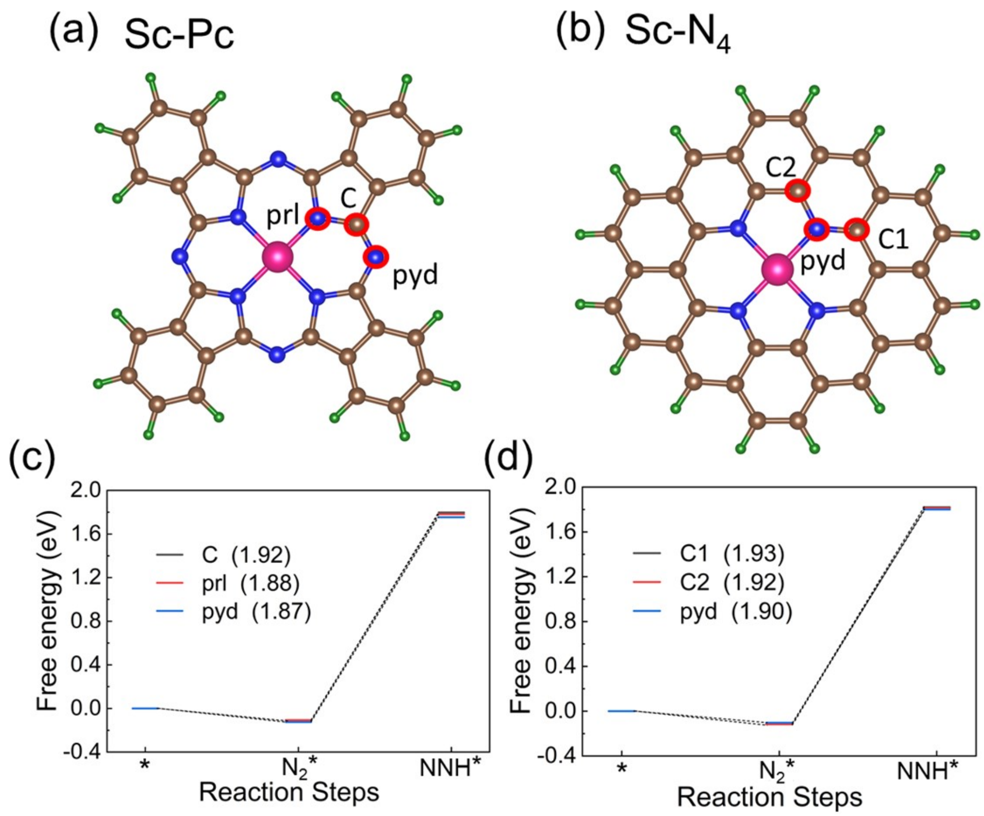

Figure S9: Structures, active sites (marked with red circled), free energy profile of N_2 and NNH adsorption on the sites of (a, c) Sc-Pc (b, d) Sc-N_4 systems. The corresponding values of eNRR overpotentials of the sites are given in parentheses in the figure legends.

SI-13. Free energy profile of N_2 and NNH adsorption on the N, C sites of Sc-N_3 and Pc systems.

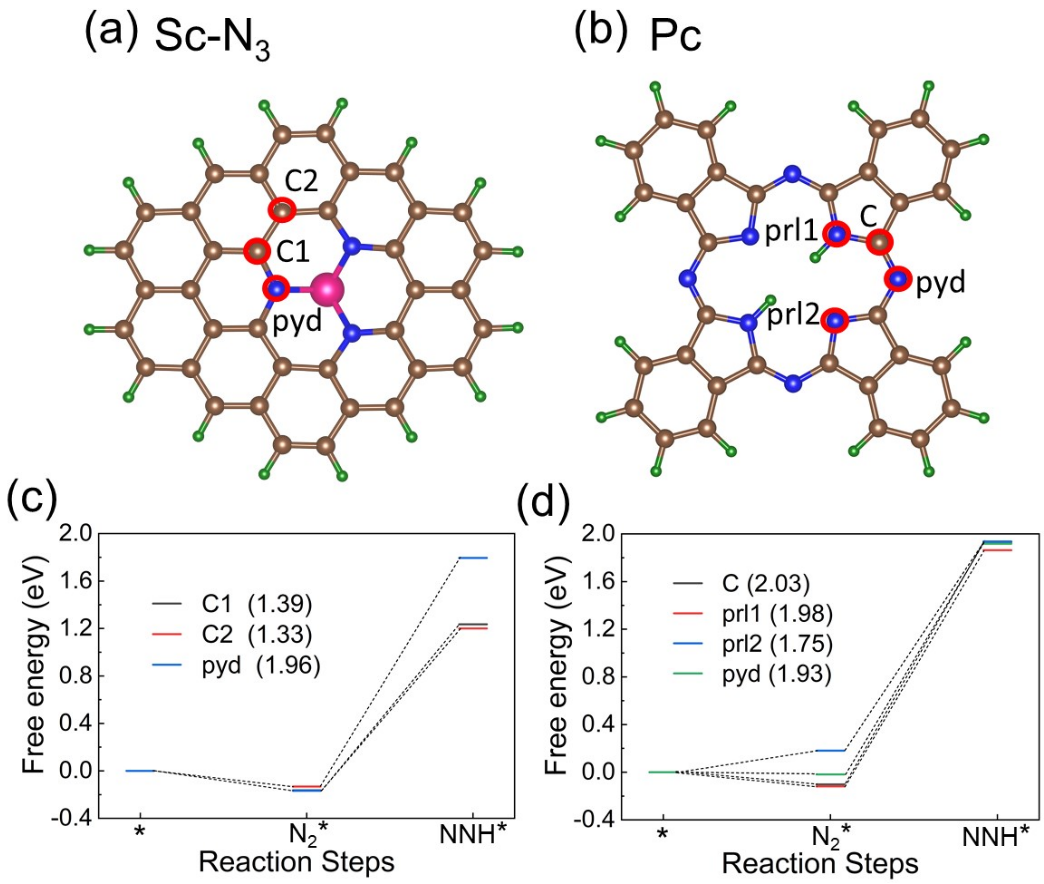

Figure S10: Structures, active sites (marked with red circled), free energy profile of N_2 and NNH adsorption on the sites of (a, b) Sc-N_3 (c, d) Pc systems. The corresponding values of eNRR overpotentials of the sites are given in parentheses in the figure legends.

SI-14. Free energy profile of N_2 and NNH adsorption on the N, C sites of Co-Pc and Ni-Pc systems.

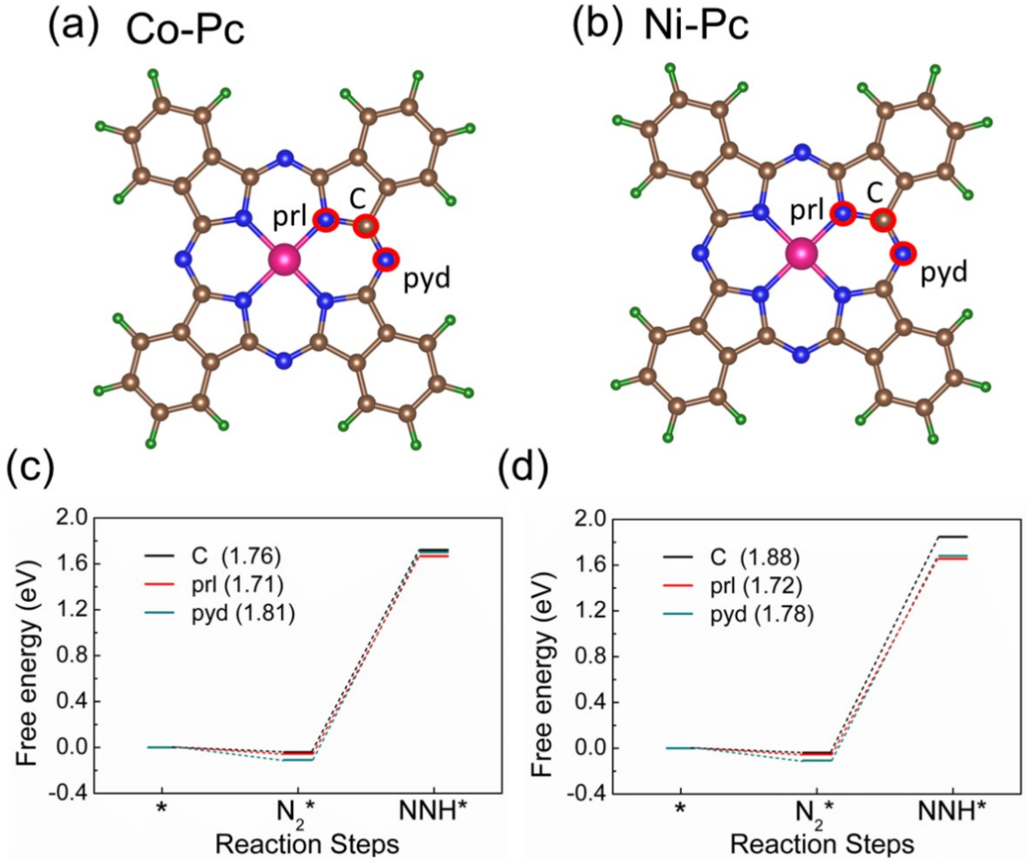

Figure S11: Structures, active sites (marked with red circled), free energy profile of N_2 and NNH adsorption on the sites of (a, c) Co-Pc (b, d) Ni-Pc systems. The corresponding values of eNRR overpotentials of the sites are given in parentheses in the figure legends.

SI-15. Free energy profile of N_2 and NNH adsorption on the Sc-Pc (Cl) and V-Pc (Cl) SACs.

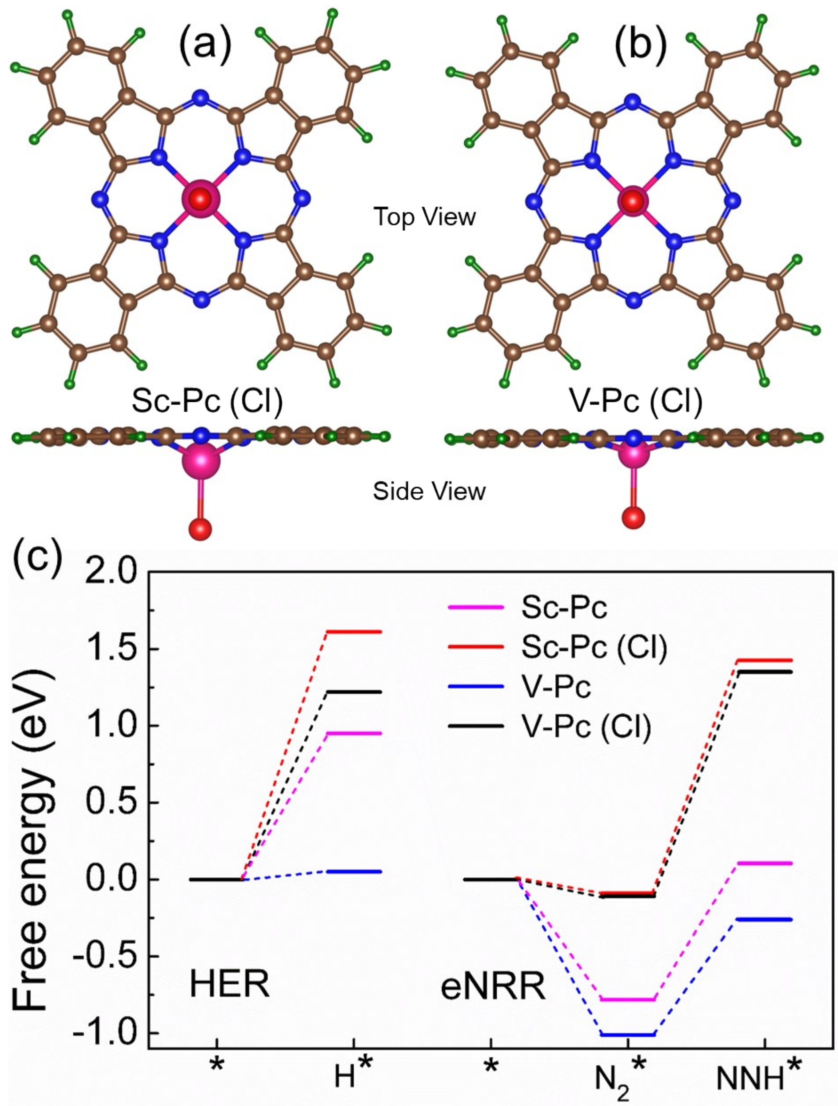

Figure S12: Optimized structures (Top view and Side view) of (a) Sc-Pc (Cl) (b) V-Pc (Cl) (c) Comparison of computed free energy profiles of H, N_2 and NNH adsorption on the Sc-Pc, Sc-Pc (Cl), V-Pc, V-Pc (Cl) SACs.

SI-16. Graph of η_{NRR} versus d band center and Bader charge.

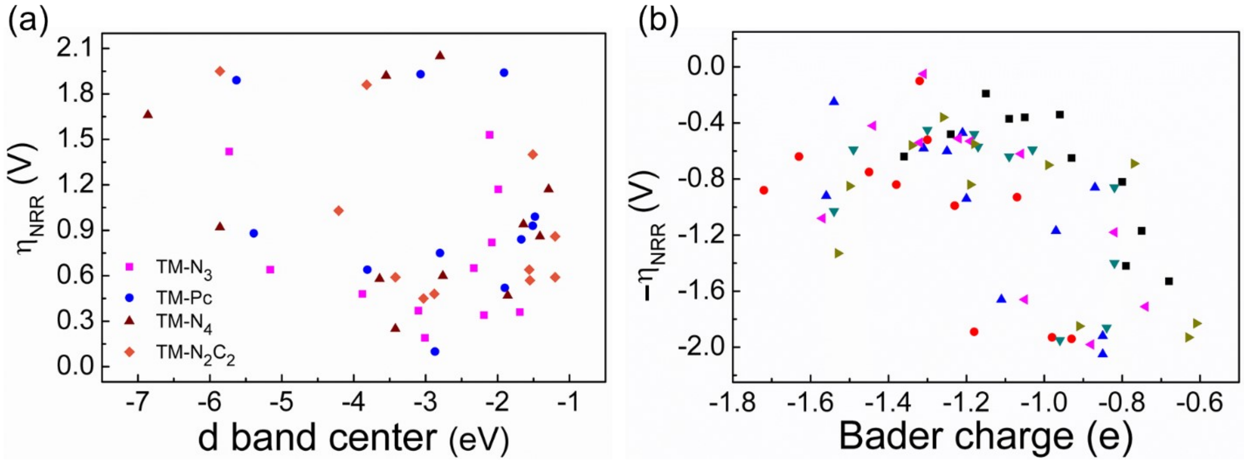

Figure S13: Poor correlation seen when plotting (a) η_NRR vs d band center and (b) -η_NRR vs Bader charge (net charge on metal center).

SI-17. Comparison of charge density differences in Mn-Pc, Mn-N_XC_Y and Mn-N_3 systems.

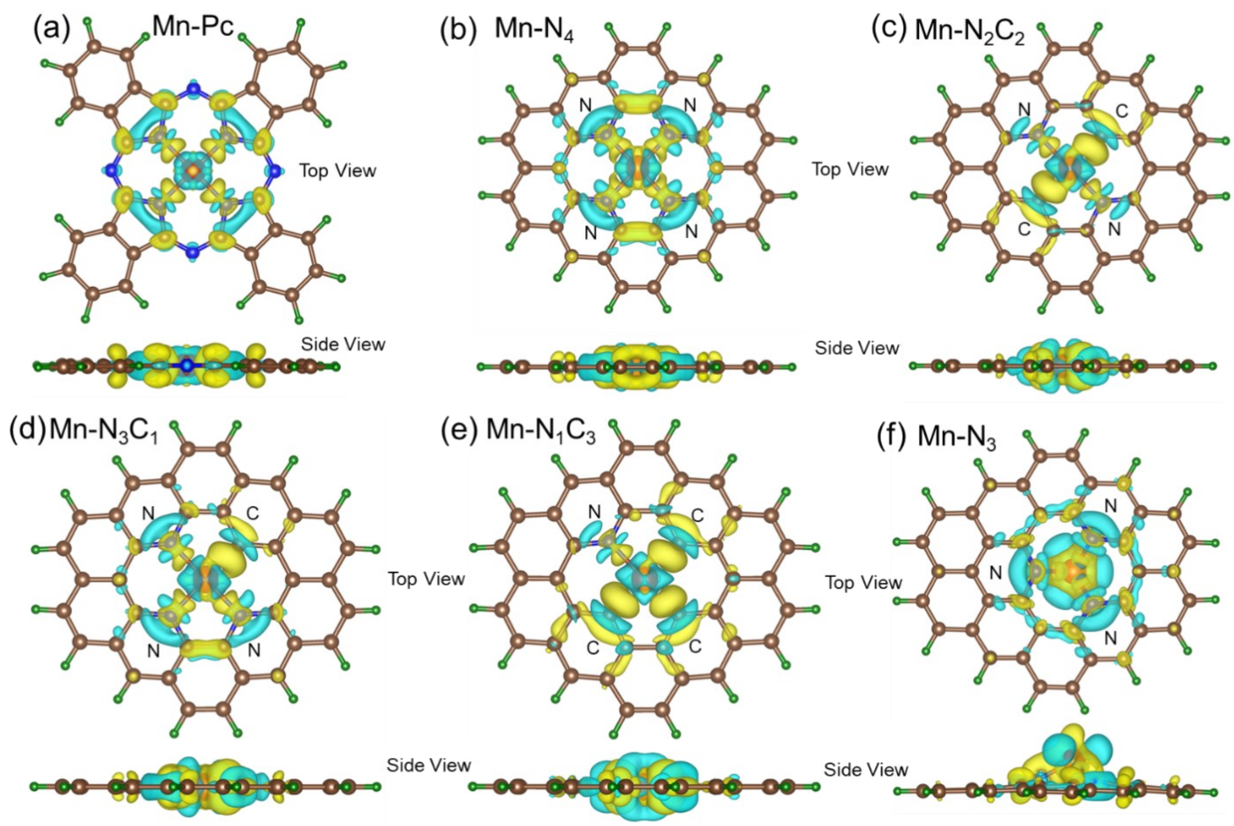

Figure S14: Charge density difference plots, indicating top and side views of the electronic redistribution that occurs on embedding the metal center within the molecule, for (a) Mn-Pc (b)

Mn-N_4 (c) Mn-N_2C_2 (d) Mn-N_3C_1 (e) Mn-N_1C_3 and (f) Mn-N_3. The symbols N and C indicate the coordination configuration. Yellow and blue lobes indicate electron accumulation and depletion, respectively (Isosurface value = 0.0032 e/Å^3).

SI-18. Comparison of charge density differences in TM-Pc systems with various metal centers.

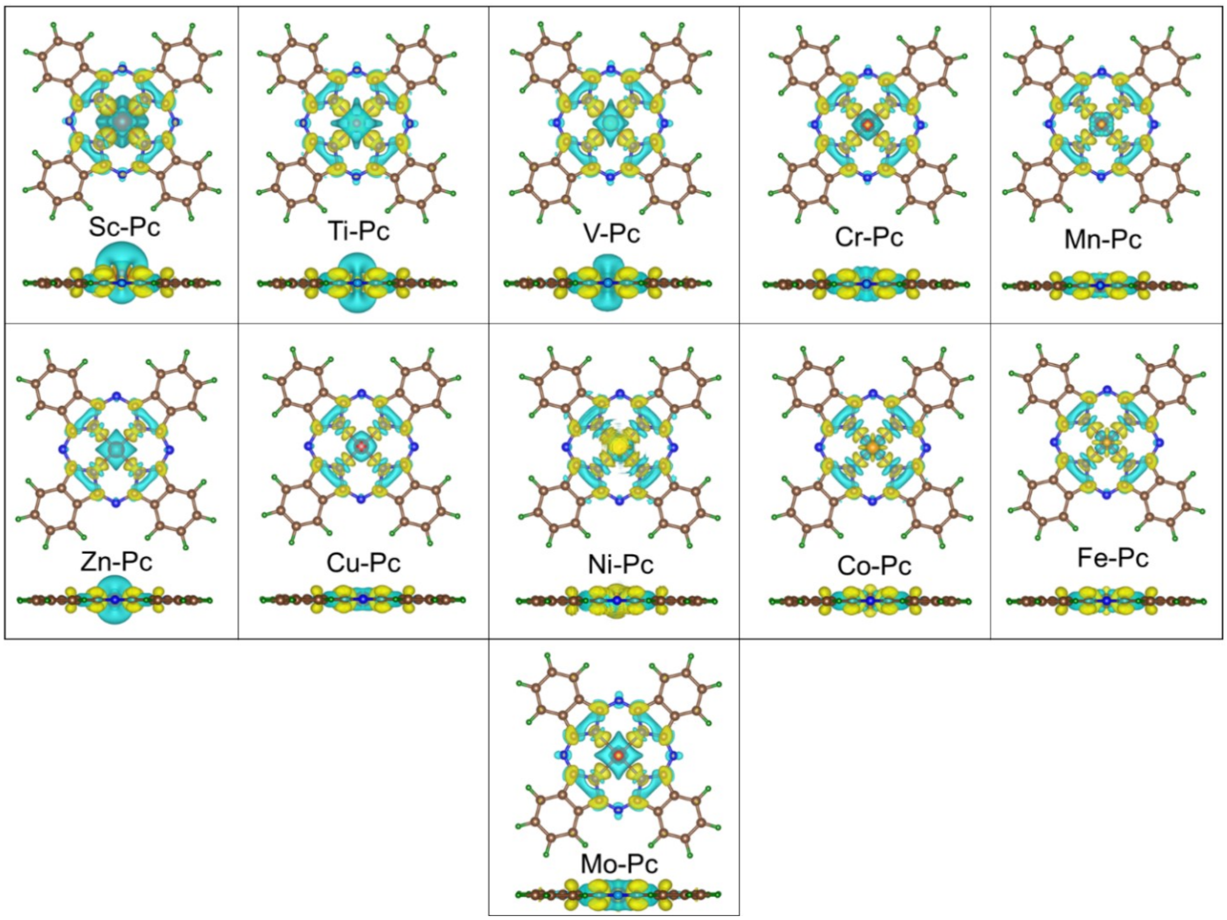

Figure S15: Charge density difference plots, indicating top and side views of the electronic redistribution that occurs on embedding the metal circle within the molecule, for Mn-Pc, with 11 different metal centers. Yellow and blue lobes indicate electron accumulation and depletion, respectively (Isosurface value = 0.0032 e/Å^3).

SI-19. The ΔG_{NNH*} Vs N-N bond length.

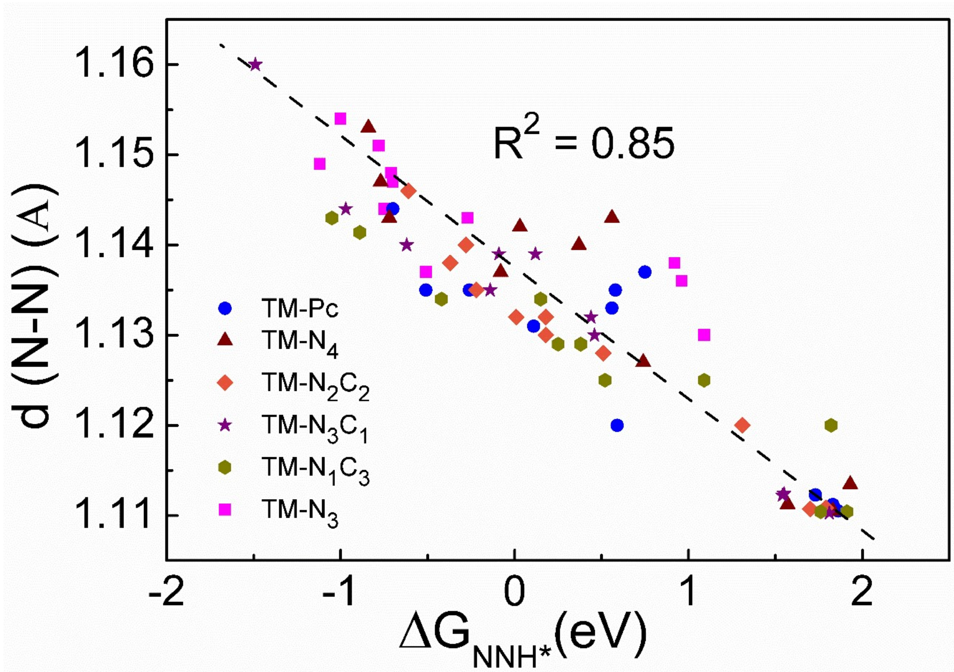

Figure S16 Correlation between ΔG_{NNH*} and N-N bond length for all 66 SACs.

SI-20. Charge density difference plots for N_2 adsorbed on different metal centers in TM-Pc.

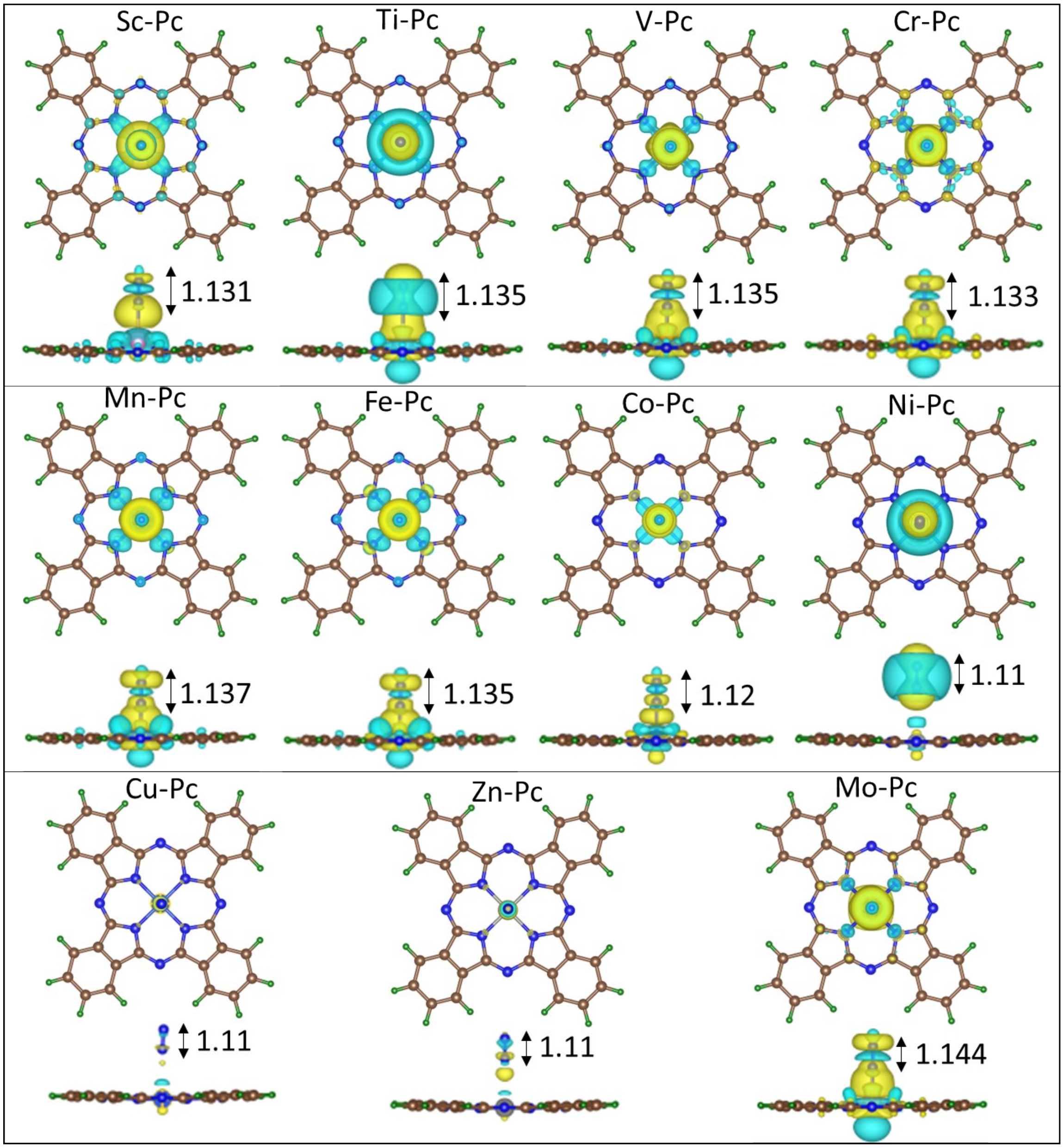

Figure S17 Charge density difference plots, indicating top and side views of the electronic redistribution that occurs due to N_2 adsorption on 11 different metal center based TM-Pc systems. Yellow and blue lobes indicate electron accumulation and depletion, respectively (Isosurface value = 0.001 e/Å^3).

SI-21. Free energy profile of the hydrogen evolution reaction for all 66 SACs.

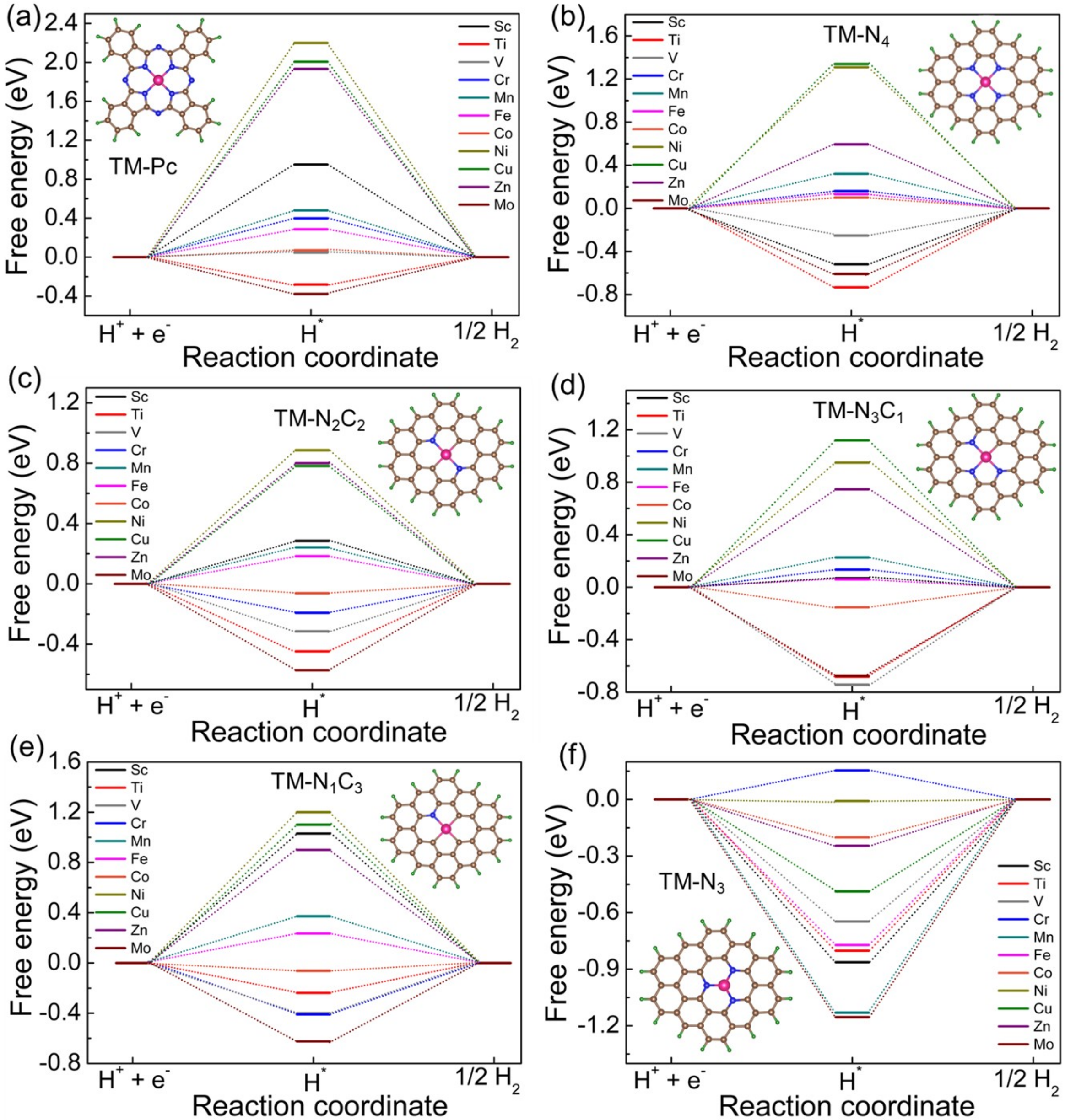

Figure S18: Computed free energy diagrams for HER (Volmer step) on various metal centers of (a) TM-Pc (b) TM-N_4 (c) TM-N_2C_2 (d) TM-N_3C_1 (e) TM-N_1C_3 and (f) TM-N_3. The dotted lines are a guide to the eye.

SI-22. Comparison of (a) $\Delta G_{N_2^*}$ and (b) ΔG_{NNH^*} for all metal centers of all 66 SACs.

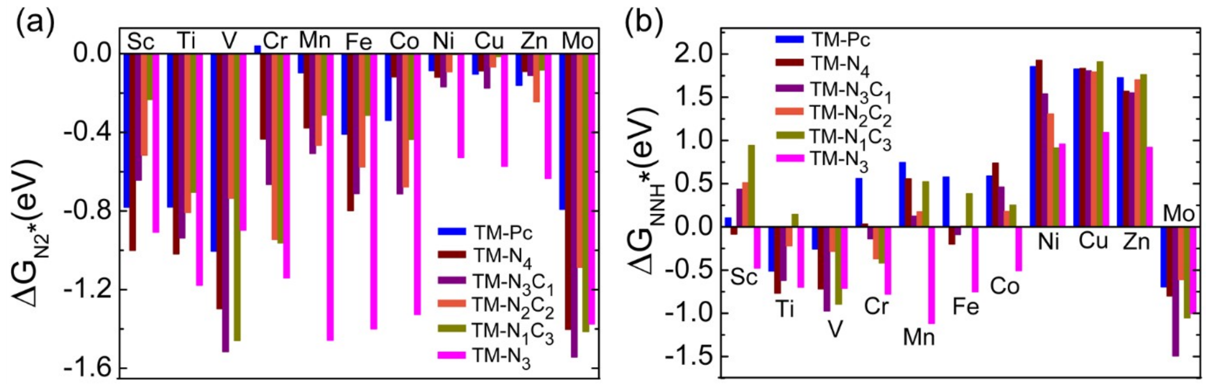

Figure S19: Bar charts showing computed values of (a) $\Delta G_{N_2^*}$ and (b) ΔG_{NNH^*} for each metal center; data are presented for all 66 SACs considered in this study.

SI-23. Flowchart of catalyst screening process.

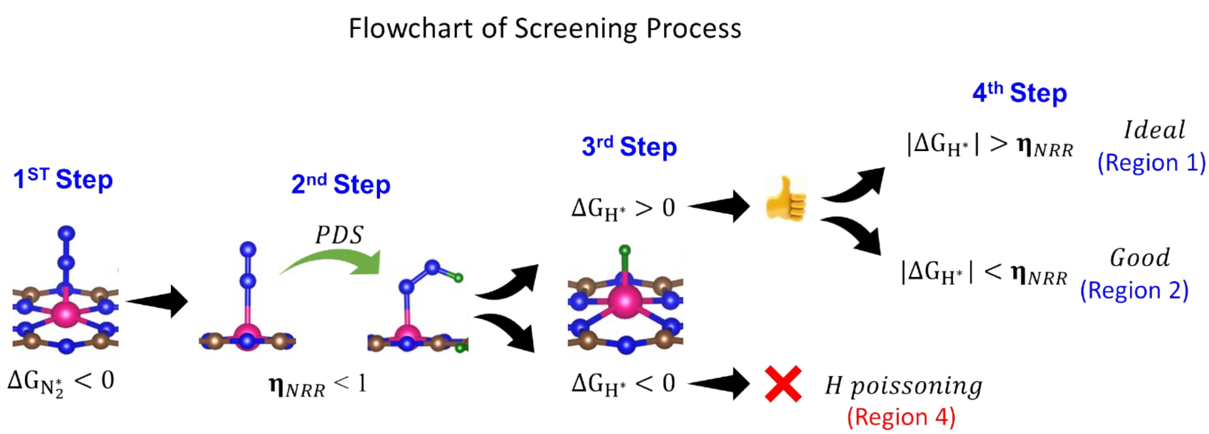

Figure S20: Flowchart of screening process of the catalysts for eNRR.

SI-24. Full free energy profile of eNRR on Cr-N_4 with and without water solvation effect.

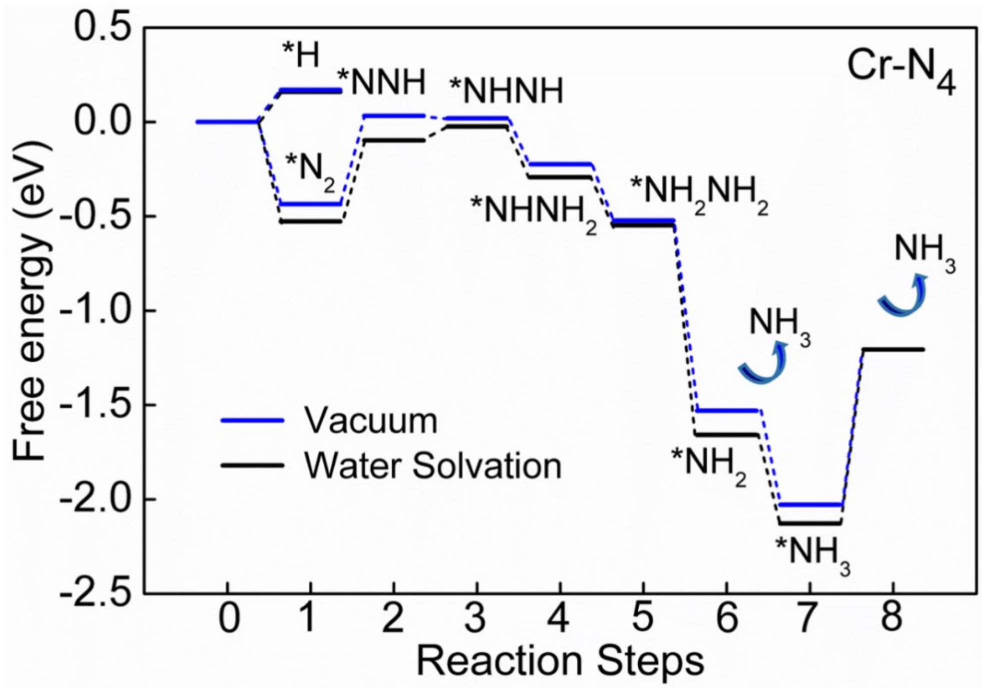

Figure S21: Full free energy profile of eNRR on Cr-N_4 SAC, in vacuum and in the presence of an implicit water solvent.

SI-25. Table of values of computed parameters for SACs

Table S1: Computed values of change in adsorption free energy of N_2 ($\Delta G_{N_2^*}$), NNH (ΔG_{NNH^*}) and hydrogen (ΔG_{H^*}) as well as the values of overpotential (η_{NRR}), Valence electron occupancy (**O**$_{val}$), formation energy ($\boldsymbol{E_f}$) (considering metal source energy from bulk and adatom) and **Region** in Figure 5b of all 66 SAC systems.

Sr. no.	**SAC**	$\Delta G_{N_2^*}$ (eV)	ΔG_{NNH^*} (eV)	η_{NRR} (V)	ΔG_{H^*} (eV)	**Valence electron occupancy (O$_{val}$)** (e)	$\boldsymbol{E_f}$ **(bulk)**	$\boldsymbol{E_f}$ **(adatom)**	**Region**
1	Sc-Pc	-0.78	0.11	0.88	0.95	1.28	-9.84	-14.18	1
2	Ti-Pc	-1.16	-0.51	0.64	-0.28	2.37	-8.76	-14.79	5
3	V-Pc	-1.01	-0.26	0.75	0.05	3.55	-8.26	-13.78	2

4	Cr-Pc	0.04	0.56	0.52	0.40	4.70	-8.83	-12.99	2
5	Mn-Pc	-0.10	0.75	0.84	0.48	5.62	-8.55	-12.55	2
6	Fe-Pc	-0.42	0.58	0.99	0.29	6.77	-7.89	-13.30	2
7	Co-Pc	-0.35	0.59	0.93	0.07	7.93	-8.03	-13.82	2
8	Ni-Pc	-0.09	1.86	1.94	2.20	9.07	-8.28	-13.30	3
9	Cu-Pc	-0.10	1.83	1.93	2.01	10.02	-7.02	-10.88	3
10	Zn-Pc	-0.16	1.73	1.89	1.93	10.82	-8.27	-9.37	3
11	Mo-Pc	-0.79	-0.70	0.10	-0.38	4.68	-6.63	-15.00	4
12	Sc-N_4	-1.00	-0.08	0.92	-0.52	1.44	-3.67	-8.00	5
13	Ti-N_4	-1.02	-0.77	0.25	-0.73	2.46	-2.36	-8.39	4
14	V-N_4	-1.30	-0.72	0.58	-0.25	3.69	-1.83	-7.35	5
15	Cr-N_4	-0.43	0.03	0.47	0.16	4.79	-2.42	-6.58	2
16	Mn-N_4	-0.38	0.56	0.94	0.32	5.80	-2.47	-6.47	2
17	Fe-N_4	-0.80	0.37	1.17	0.13	7.03	-2.14	-7.55	3
18	Co-N_4	-0.12	0.74	0.86	0.10	8.13	-2.58	-8.37	2
19	Ni-N_4	-0.12	1.93	2.05	1.31	9.15	-2.59	-7.61	3
20	Cu-N_4	-0.09	1.83	1.92	1.34	10.15	-1.15	-5.00	3
21	Zn-N_4	-0.09	1.57	1.66	0.59	10.89	-2.27	-3.37	3
22	Mo-N_4	-1.40	-0.84	0.60	-0.61	4.75	0.40	-7.92	4
23	Sc-N_2C_2	-0.52	0.51	1.03	0.28	1.46	-1.16	-5.50	3
24	Ti-N_2C_2	-0.81	-0.22	0.59	-0.45	2.51	-0.50	-6.53	5
25	V-N_2C_2	-0.74	-0.28	0.45	-0.32	3.70	0.35	-5.17	5
26	Cr-N_2C_2	-0.95	-0.37	0.57	-0.19	4.83	0.51	-3.66	5
27	Mn-N_2C_2	-0.47	0.18	0.64	0.24	5.91	-0.13	-4.13	2
28	Fe-N_2C_2	-0.58	0.01	0.59	0.18	6.97	0.29	-5.12	2
29	Co-N_2C_2	-0.68	0.18	0.86	-0.06	8.18	-0.06	-5.86	5
30	Ni-N_2C_2	-0.09	1.31	1.40	0.89	9.18	-0.55	-5.58	3

31	Cu-N_2C_2	-0.07	1.79	1.86	0.78	10.16	0.57	-3.29	3
32	Zn-N_2C_2	-0.24	1.70	1.95	0.80	11.04	0.29	-0.81	3
33	Mo-N_2C_2	-1.09	-0.61	0.48	-0.57	4.82	1.44	-6.88	4
34	Sc-N_3C_1	-0.64	0.44	1.08	0.07	1.43	-2.69	-7.02	3
35	Ti-N_3C_1	-1.04	-0.62	0.42	-0.68	2.56	-1.45	-7.48	4
36	V-N_3C_1	-1.52	-0.97	0.54	-0.74	3.68	-0.32	-5.84	4
37	Cr-N_3C_1	-0.67	-0.14	0.53	0.13	4.81	-1.03	-5.20	2
38	Mn-N_3C_1	-0.38	0.12	0.51	0.23	5.78	-1.40	-5.40	2
39	Fe-N_3C_1	-0.71	-0.09	0.62	0.06	6.94	-1.00	-6.40	2
40	Co-N_3C_1	-0.71	0.46	1.18	-0.15	8.18	-1.41	-7.21	5
41	Ni-N_3C_1	-0.17	1.54	1.71	0.95	9.26	-1.79	-6.82	3
42	Cu-N_3C_1	-0.18	1.81	1.98	1.12	10.12	-0.29	-4.14	3
43	Zn-N_3C_1	-0.11	1.55	1.66	0.75	10.95	-0.89	-1.98	3
44	Mo-N_3C_1	-1.54	-1.49	0.05	-0.67	4.69	2.00	-6.32	4
45	Sc-N_1C_3	-0.23	1.09	1.33	1.03	1.47	0.28	-4.05	3
46	Ti-N_1C_3	-0.71	0.15	0.85	-0.24	2.50	0.65	-5.38	5
47	V-N_1C_3	-1.46	-0.89	0.56	-0.40	3.66	2.17	-3.35	5
48	Cr-N_1C_3	-0.96	-0.42	0.55	-0.41	4.82	1.96	-2.20	5
49	Mn-N_1C_3	-0.31	0.52	0.84	0.37	5.81	0.81	-3.19	2
50	Fe-N_1C_3	-0.31	0.38	0.70	0.23	7.01	1.28	-4.13	2
51	Co-N_1C_3	-0.44	0.25	0.69	-0.06	8.23	1.19	-4.60	5
52	Ni-N_1C_3	-0.01	1.82	1.83	1.20	9.39	0.79	-4.24	3
53	Cu-N_1C_3	-0.01	1.91	1.93	1.11	10.37	0.88	-2.98	3
54	Zn-N_1C_3	-0.08	1.76	1.85	0.90	11.09	1.41	0.32	3
55	Mo-N_1C_3	-1.41	-1.05	0.36	-0.62	4.74	3.83	-4.49	4
56	Sc-N_3	-0.91	-0.27	0.64	-0.86	1.64	-1.97	-6.31	4
57	Ti-N_3	-1.18	-0.70	0.48	-0.80	2.76	-0.86	-6.89	4

58	V-N_3	-0.90	-0.71	0.19	-0.65	3.85	-0.43	-5.95	4
59	Cr-N_3	-1.14	-0.78	0.36	0.15	4.95	0.28	-3.88	2
60	Mn-N_3	-1.46	-1.12	0.34	-1.13	6.04	0.41	-3.59	4
61	Fe-N_3	-1.40	-0.75	0.65	-0.77	7.07	0.65	-4.76	4
62	Co-N_3	-1.33	-0.51	0.82	-0.20	8.20	0.02	-5.78	5
63	Ni-N_3	-0.53	0.96	1.17	-0.01	9.25	0.29	-4.74	5
64	Cu-N_3	-0.57	1.09	1.53	-0.49	10.32	0.46	-3.40	5
65	Zn-N_3	-0.63	0.92	1.42	-0.25	11.21	-0.57	-1.66	5
66	Mo-N_3	-1.37	-1.00	0.37	-1.15	4.91	1.90	-6.42	4

SI-26. The values of $\Delta G_{N_2^*}$ with end-on and side-on configuration on the metal site of all 66 SACs.

Table S2 Computed values of $\Delta G_{N_2^*}$ in both Endon and Sideon configuration for all 66 SACs. The SACs represented with coloured shows lower N_2 adsorption energy with side-on form than end-on configuration.

Sr. no.	**SAC**	$\Delta G_{N_2^*}$ $(Endon)$ (eV)	$\Delta G_{N_2^*}$ $(Sideon)$ (eV)	**SAC**	$\Delta G_{N_2^*}$ $(Endon)$ (eV)	$\Delta G_{N_2^*}$ $(Sideon)$ (eV)
1	Sc-Pc	-0.78	-0.66	Sc-N_4	-1.00	-0.62
2	Ti-Pc	-1.16	-0.73	Ti-N_4	-1.02	-0.89
3	V-Pc	-1.01	-0.24	V-N_4	-1.30	-0.61
4	Cr-Pc	0.04	0.76	Cr-N_4	-0.43	1.42
5	Mn-Pc	-0.10	1.01	Mn-N_4	-0.38	-0.07
6	Fe-Pc	-0.42	-0.21	Fe-N_4	-0.80	0.15

7	Co-Pc	-0.35	-0.06	Co-N_4	-0.12	-0.08
8	Ni-Pc	-0.09	-0.06	Ni-N_4	-0.12	-0.09
9	Cu-Pc	-0.10	-0.01	Cu-N_4	-0.09	-0.06
10	Zn-Pc	-0.16	-0.07	Zn-N_4	-0.09	-0.04
11	Mo-Pc	-0.79	-0.21	Mo-N_4	-1.40	-1.57
Sr. no.	**SAC**	$\Delta G_{N_2^*}$ $(Endon)$ (eV)	$\Delta G_{N_2^*}$ $(Sideon)$ (eV)	**SAC**	$\Delta G_{N_2^*}$ $(Endon)$ (eV)	$\Delta G_{N_2^*}$ $(Sideon)$ (eV)
1	Sc-N_2C_2	-0.52	-0.23	Sc-N_3C_1	-0.64	-0.37
2	Ti-N_2C_2	-0.81	-0.60	Ti-N_3C_1	-1.04	-0.96
3	V-N_2C_2	-0.74	-0.58	V-N_3C_1	-1.52	-1.35
4	Cr-N_2C_2	-0.95	-0.70	Cr-N_3C_1	-0.67	-0.09
5	Mn-N_2C_2	-0.47	0.03	Mn-N_3C_1	-0.38	0.19
6	Fe-N_2C_2	-0.58	-0.10	Fe-N_3C_1	-0.71	0.13
7	Co-N_2C_2	-0.68	0.14	Co-N_3C_1	-0.71	-0.69
8	Ni-N_2C_2	-0.09	-0.08	Ni-N_3C_1	-0.17	-0.10
9	Cu-N_2C_2	-0.07	-0.05	Cu-N_3C_1	-0.18	-0.11
10	Zn-N_2C_2	-0.24	-0.23	Zn-N_3C_1	-0.11	-0.10
11	Mo-N_2C_2	-1.09	-0.98	Mo-N_3C_1	-1.54	-2.44
Sr. no.	**SAC**	$\Delta G_{N_2^*}$ $(Endon)$ (eV)	$\Delta G_{N_2^*}$ $(Sideon)$ (eV)	**SAC**	$\Delta G_{N_2^*}$ $(Endon)$ (eV)	$\Delta G_{N_2^*}$ $(Sideon)$ (eV)
1	Sc-N_1C_3	-0.23	-0.17	Sc-N_3	-0.91	-1.05

2	Ti-N_1C_3	-0.71	-0.48	Ti-N_3	-1.18	-1.28
3	V-N_1C_3	-1.46	-1.24	V-N_3	-0.90	-1.04
4	Cr-N_1C_3	-0.96	-0.73	Cr-N_3	-1.14	-1.13
5	Mn-N_1C_3	-0.31	-0.01	Mn-N_3	-1.46	-1.53
6	Fe-N_1C_3	-0.31	0.21	Fe-N_3	-1.40	-1.51
7	Co-N_1C_3	-0.44	0.03	Co-N_3	-1.33	-0.82
8	Ni-N_1C_3	-0.01	0.00	Ni-N_3	-0.53	-0.43
9	Cu-N_1C_3	-0.01	0.03	Cu-N_3	-0.57	-0.36
10	Zn-N_1C_3	-0.08	-0.08	Zn-N_3	-0.63	-0.09
11	Mo-N_1C_3	-1.41	-2.45	Mo-N_3	-1.37	-1.88

SI-27. The N-N bond length after adsorption on SACs.

Table S3 The computed values of N-N bond length in all 66 N_2 adsorbed SACs. The unit of bond length is Å.

Sr. no.	**SAC**	$d\,(N{-}N)$	**SAC**	$d\,(N{-}N)$	**SAC**	$d\,(N{-}N)$
1	Sc-Pc	1.131	Sc-N_4	1.137	Sc-N_2C_2	1.128
2	Ti-Pc	1.135	Ti-N_4	1.147	Ti-N_2C_2	1.135
3	V-Pc	1.135	V-N_4	1.143	V-N_2C_2	1.14
4	Cr-Pc	1.133	Cr-N_4	1.142	Cr-N_2C_2	1.138
5	Mn-Pc	1.137	Mn-N_4	1.143	Mn-N_2C_2	1.13
6	Fe-Pc	1.135	Fe-N_4	1.14	Fe-N_2C_2	1.132
7	Co-Pc	1.12	Co-N_4	1.127	Co-N_2C_2	1.132
8	Ni-Pc	1.11	Ni-N_4	1.11	Ni-N_2C_2	1.12

9	Cu-Pc	1.11	Cu-N_4	1.11	Cu-N_2C_2	1.11
10	Zn-Pc	1.11	Zn-N_4	1.11	Zn-N_2C_2	1.11
11	Mo-Pc	1.144	Mo-N_4	1.153	Mo-N_2C_2	1.146

Sr. no.	**SAC**	$d\,(N{-}N)$	**SAC**	$d\,(N{-}N)$	**SAC**	$d\,(N{-}N)$
1	Sc-N_3C_1	1.132	Sc-N_1C_3	1.125	Sc-N_3	1.143
2	Ti-N_3C_1	1.14	Ti-N_1C_3	1.134	Ti-N_3	1.147
3	V-N_3C_1	1.144	V-N_1C_3	1.1414	V-N_3	1.148
4	Cr-N_3C_1	1.135	Cr-N_1C_3	1.13	Cr-N_3	1.151
5	Mn-N_3C_1	1.139	Mn-N_1C_3	1.125	Mn-N_3	1.149
6	Fe-N_3C_1	1.139	Fe-N_1C_3	1.129	Fe-N_3	1.144
7	Co-N_3C_1	1.13	Co-N_1C_3	1.129	Co-N_3	1.137
8	Ni-N_3C_1	1.11	Ni-N_1C_3	1.12	Ni-N_3	1.136
9	Cu-N_3C_1	1.11	Cu-N_1C_3	1.11	Cu-N_3	1.13
10	Zn-N_3C_1	1.11	Zn-N_1C_3	1.11	Zn-N_3	1.138
11	Mo-N_3C_1	1.16	Mo-N_1C_3	1.143	Mo-N_3	1.154

SI-28. The comparison of NH_3 yield and FE of SACs by using reported experimental studies.

Table S4: The reported experimental studies on the electrochemical performance (NH_3 yield and FE) of our proposed SACs from different regions of Figure 5.

Experimental			**Theoretical** (Figure 5)			
Catalyst	**Yield rate** μg h^{-1} mg^{-1}_{cat}	**FE %** V vs RHE	$\Delta G_{N_2^*}$ (eV)	η_{NRR} (V)	ΔG_{H^*} (eV)	**Region**

Co-Pc [9]	**107.9**	**27.7** at -0.3	-0.35	0.93	+0.07	2
Fe-Pc [10]	**137.95**	**10.5** at -0.3	-0.42	0.99	+0.29	2
$Mn-N_4$ [11]	**67.5**	**13.7** at -0.25	-0.38	0.94	+0.32	2
$Fe-N_4$ [12]	**62.9**	**18.6** at -0.4	-0.80	1.17	+0.13	2
$Cu-N_4$ [13]	49.3	11.7 at -0.3	-0.09	1.92	+1.34	3
$Mo-N_3$ [14]	31.5	6.8 at -0.25	-1.37	0.37	-1.15	4
$Mo-N_4$ [15]	1.8	1.5 at -0.2	-1.40	0.60	-0.61	4
$Co-N_3$ [16]	37.6	7.6 at -0.9	-1.33	0.82	-0.20	4
$Mn-N_3$ [17]	21.43	8.8 at -0.65	-1.46	0.34	-1.13	4

Region 2: less H poisoning, low HER, high NH_3 yield rate and FE for eNRR.

Region 4: High H poisoning, HER favourable, low NH_3 yield rate and FE for eNRR.

SI-29. Values of U_{diss}, U^0_{diss}, $and\ n$.

Table S5: The values of U_{diss}, U^0_{diss}, n for all 66 SAC system.

Sr. no.	SAC	U^0_{diss}	n	U_{diss} (bulk)	U_{diss} (adatom)
1	Sc-Pc	-2.08	3	1.20	2.65
2	Ti-Pc	-1.63	2	2.75	5.77
3	V-Pc	-1.18	2	2.95	5.71
4	Cr-Pc	-0.91	2	3.50	5.59
5	Mn-Pc	-1.19	2	3.09	5.09
6	Fe-Pc	-0.45	2	3.50	6.20
7	Co-Pc	-0.28	2	3.73	6.63
8	Ni-Pc	-0.26	2	3.88	6.39
9	Cu-Pc	0.34	2	3.85	5.78
10	Zn-Pc	-0.76	2	3.38	3.93
11	Mo-Pc	-0.2	3	2.01	4.80
12	$Sc-N_4$	-2.08	3	-0.86	0.59

13	Ti-N_4	-1.63	2	-0.45	2.57
14	V-N_4	-1.18	2	-0.27	2.50
15	Cr-N_4	-0.91	2	0.30	2.38
16	Mn-N_4	-1.19	2	0.05	2.05
17	Fe-N_4	-0.45	2	0.62	3.33
18	Co-N_4	-0.28	2	1.01	3.91
19	Ni-N_4	-0.26	2	1.04	3.55
20	Cu-N_4	0.34	2	0.92	2.84
21	Zn-N_4	-0.76	2	0.38	0.93
22	Mo-N_4	-0.2	3	-0.33	2.44
23	Sc-N_2C_2	-2.08	3	-1.69	-0.25
24	Ti-N_2C_2	-1.63	2	-1.38	1.64
25	V-N_2C_2	-1.18	2	-1.36	1.41
26	Cr-N_2C_2	-0.91	2	-1.17	0.92
27	Mn-N_2C_2	-1.19	2	-1.13	0.88
28	Fe-N_2C_2	-0.45	2	-0.60	2.11
29	Co-N_2C_2	-0.28	2	-0.25	2.65
30	Ni-N_2C_2	-0.26	2	0.02	2.53
31	Cu-N_2C_2	0.34	2	0.06	1.99
32	Zn-N_2C_2	-0.76	2	-0.91	-0.36
33	Mo-N_2C_2	-0.2	3	-0.68	2.09
34	Sc-N_3C_1	-2.08	3	-1.18	0.26
35	Ti-N_3C_1	-1.63	2	-0.91	2.11
36	V-N_3C_1	-1.18	2	-1.02	1.74
37	Cr-N_3C_1	-0.91	2	-0.40	1.69
38	Mn-N_3C_1	-1.19	2	-0.49	1.51
39	Fe-N_3C_1	-0.45	2	0.05	2.75

40	$Co\text{-}N_3C_1$	-0.28	2	0.43	3.33
41	$Ni\text{-}N_3C_1$	-0.26	2	0.64	3.15
42	$Cu\text{-}N_3C_1$	0.34	2	0.49	2.41
43	$Zn\text{-}N_3C_1$	-0.76	2	-0.32	0.23
44	$Mo\text{-}N_3C_1$	-0.2	3	-0.87	1.91
45	$Sc\text{-}N_1C_3$	-2.08	3	-2.17	-0.73
46	$Ti\text{-}N_1C_3$	-1.63	2	-1.96	1.06
47	$V\text{-}N_1C_3$	-1.18	2	-2.27	0.50
48	$Cr\text{-}N_1C_3$	-0.91	2	-1.89	0.19
49	$Mn\text{-}N_1C_3$	-1.19	2	-1.60	0.41
50	$Fe\text{-}N_1C_3$	-0.45	2	-1.09	1.62
51	$Co\text{-}N_1C_3$	-0.28	2	-0.88	2.02
52	$Ni\text{-}N_1C_3$	-0.26	2	-0.66	1.86
53	$Cu\text{-}N_1C_3$	0.34	2	-0.10	1.83
54	$Zn\text{-}N_1C_3$	-0.76	2	-1.47	-0.92
55	$Mo\text{-}N_1C_3$	-0.2	3	-1.48	1.30
56	$Sc\text{-}N_3$	-2.08	3	-1.42	0.02
57	$Ti\text{-}N_3$	-1.63	2	-1.20	1.82
58	$V\text{-}N_3$	-1.18	2	-0.97	1.80
59	$Cr\text{-}N_3$	-0.91	2	-1.05	1.03
60	$Mn\text{-}N_3$	-1.19	2	-1.40	0.61
61	$Fe\text{-}N_3$	-0.45	2	-0.78	1.93
62	$Co\text{-}N_3$	-0.28	2	-0.29	2.61
63	$Ni\text{-}N_3$	-0.26	2	-0.41	2.11
64	$Cu\text{-}N_3$	0.34	2	0.11	2.04
65	$Zn\text{-}N_3$	-0.76	2	-0.48	0.07
66	$Mo\text{-}N_3$	-0.2	3	-0.83	1.94

SI-30. References

1 G. Kresse and D. Joubert, *Phys. Rev. B*, 1999, **59**, 1758–1775.

2 J. P. Perdew, K. Burke and M. Ernzerhof, *Phys. Rev. Lett.*, 1996, **77**, 3865–3868.

3 S. Bhattacharjee, U. V Waghmare and S.-C. Lee, *Sci. Rep.*, 2016, **6**, 35916.

4 W. Mtangi, V. Kiran, C. Fontanesi and R. Naaman, *J. Phys. Chem. Lett.*, 2015, **6**, 4916–4922.

5 S. Sinthika, U. V. Waghmare and R. Thapa, *Small*, , DOI:10.1002/smll.201703609.

6 P. Giannozzi, S. Baroni, N. Bonini, M. Calandra, R. Car, C. Cavazzoni, D. Ceresoli, G. L. Chiarotti, M. Cococcioni, I. Dabo, A. D. Corso, S. de Gironcoli, S. Fabris, G. Fratesi, R. Gebauer, U. Gerstmann, C. Gougoussis, A. Kokalj, M. Lazzeri, L. Martin-Samos, N. Marzari, F. Mauri, R. Mazzarello, S. Paolini, A. Pasquarello, L. Paulatto, C. Sbraccia, S. Scandolo, G. Sclauzero, A. P. Seitsonen, A. Smogunov, P. Umari and R. M. Wentzcovitch, *J. Phys. Condens. Matter*, 2009, **21**, 395502.

7 H. Yin, S.-L. Li, L.-Y. Gan and P. Wang, *J. Mater. Chem. A*, 2019, **7**, 11908–11914.

8 X. Li, Q. Zhou, S. Wang, Y. Li, Y. Liu, Q. Gao and Q. Wu, *J. Phys. Chem. C*, 2021, **125**, 11963–11974.

9 U. K. Ghorai, S. Paul, B. Ghorai, A. Adalder, S. Kapse, R. Thapa, A. Nagendra and A. Gain, *ACS Nano*, 2021, **15**, 5230–5239.

10 C. He, Z.-Y. Wu, L. Zhao, M. Ming, Y. Zhang, Y. Yi and J.-S. Hu, *ACS Catal.*, 2019, **9**, 7311–7317.

11 S. Zhoutai, S. Bin, L. Hongbao, Z. Hong, F. Fan, K. Jacob, Z. Wenli, X. Beibei, C. Yingwen, L. Ke and C. Qianwang, *CCS Chem.*, , DOI:10.31635/ccschem.021.202101106.

12 F. Lü, S. Zhao, R. Guo, J. He, X. Peng, H. Bao, J. Fu, L. Han, G. Qi, J. Luo, X. Tang and X. Liu, *Nano Energy*, 2019, **61**, 420–427.

13 W. Zang, T. Yang, H. Zou, S. Xi, H. Zhang, X. Liu, Z. Kou, Y. Du, Y. P. Feng, L. Shen, L. Duan, J. Wang and S. J. Pennycook, *ACS Catal.*, 2019, **9**, 10166–10173.

14 L. Han, X. Liu, J. Chen, R. Lin, H. Liu, F. Lü, S. Bak, Z. Liang, S. Zhao, E. Stavitski, J. Luo, R. R. Adzic and H. L. Xin, *Angew. Chemie Int. Ed.*, 2019, **58**, 2321–2325.

15 Y. Li, Q. Zhang, C. Li, H.-N. Fan, W.-B. Luo, H.-K. Liu and S.-X. Dou, *J. Mater. Chem. A*, 2019, **7**, 22242–22247.

16 M. Qin, X. Li, G. Gan, L. Wang, S. Fan, Z. Yin and G. Chen, *ACS Sustain. Chem. Eng.*, 2020, **8**, 13430–13439.

17 X. Wang, D. Wu, S. Liu, J. Zhang, X.-Z. Fu and J.-L. Luo, *Nano-Micro Lett.*, 2021, **13**, 125.